CHAPTER

14

Cause of Global Climate Changes: Correlation of Global Temperature, Sunspots, Solar Irradiance, Cosmic Rays, and Radiocarbon and Berylium Production Rates

D.J. Easterbrook

Western Washington University, Bellingham, WA, United States

OUTLINE

1. SOLAR VARIATION—GRAND MINIMA

At the end of the Medieval Warm Period, ~1300 AD, temperatures dropped dramatically and the cold period that followed is known as the Little Ice Age. The periods of colder climate that ensued for five centuries were devastating. The population of Europe had become dependent on cereal grains as a food supply during the Medieval Warm Period, and with the colder climate, early snows, violent storms, and recurrent flooding that swept Europe, massive crop failures occurred, resulting in widespread famine and disease (Fagan, 2000; Grove, 2004). Glaciers in Greenland and elsewhere began advancing and pack ice extended southward in the North Atlantic, blocking ports and affecting fishing. Three years of torrential rains that began in 1315 led to the Great Famine of 1315–1317.

Evidence-Based Climate Science, Second Edition
http://dx.doi.org/10.1016/B978-0-12-804588-6.00014-8

The Little Ice Age was not a time of continuous cold climate, but rather repeated periods of cooling and warming, each of which occurred during times of solar minima, characterized by low sunspot numbers, low total solar irradiance (TSI), decreased solar magnetism, increased cosmic ray intensity, and increased production of radiocarbon and beryllium in the upper atmosphere.

Centuries of observations of the sun have shown that sunspots, solar irradiance, and solar magnetism vary over time, and these phenomena correlate very well with global climate changes on Earth. A number of solar Grand Minima, periods of reduced solar output, have been recognized (Fig. 14.1).

1.1 Wolf Minimum (1290–1320 AD)

The Wolf Minimum was a period of low sunspot numbers (SSNs) and TSI between about 1300 and 1320 AD. It occurred during the cold period that marked the end of the Medieval Warm Period (MWP) and the beginning of the Little Ice Age (LIA) about 1300 AD.

The change from the warmth of the MWP to the cold of the LIA was abrupt and devastating, leading to the Great Famine from 1310 to 1322. The winter of 1309–1310 AD was exceptionally cold. The Thames River froze over and poor people were especially affected. The year 1315 AD was especially bad. Jean Desnouelles wrote at the time, "Exceedingly great rains descended from the heavens and they made huge and deep mud-pools on the land. Throughout nearly all of May, June, and August, the rains did not stop." Corn, oats, and hay crops were beaten to the ground, August and September were cold, and floods swept away entire villages. Crop harvests in 1315 AD were a disaster, affecting an enormous area in northern Europe. In places, up to half of farmlands were eroded away, cold, wet weather prevented grain harvests, and fall plantings failed, triggering famines.

In 1316 AD, spring rain continued, again impeding the sowing of grain crops, and harvests failed once again. Diseases increased, newborn and old people died of starvation, and multitudes scavenged anything edible. Whole communities disappeared and many farms were abandoned. The year 1316 was the worst for cereal crops in the entire Middle Ages. Cattle couldn't be fed, hay wouldn't dry and couldn't be moved so it just rotted. Thousands of cattle froze during the bitterly cold winter of 1317–1318 and many others starved. The cold immobilized shipping. Rain in 1317–1318 continued through the summer and people suffered for another seven years. The coincidence of sudden cooling of the climate from the warm Medieval Warm Period to the harsh cold climate of the Little Ice Age during the Wolf Minimum was not just a coincidence, as shown by at least five later, similar instances.

1.2 Sporer Minimum (1410–1540)

The Sporer Minimum occurred from about 1410 to 1540 (Fig. 14.1). Like the Wolf Minimum, the Sporer coincided with a cold period (Fig. 14.2).

1.3 Maunder Minimum

The Maunder Minimum is the most famous cold period of the Little Ice Age. Temperatures plummeted in Europe (Figs. 14.3–14.7), the growing season became shorter by more than a month, the number of snowy days increased

Selected solar activity events

Event	Approx dates	
Medieval maximum	1100	1250
Wolf minimum	1280	1350
Spörer Minimum	1460	1550
Maunder Minimum	1645	1715
Dalton Minimum	1790	1820
1880-1915 Minimum	1880	1915
1945-1977 Minimum	1945	1977

FIGURE 14.1 Solar minima.

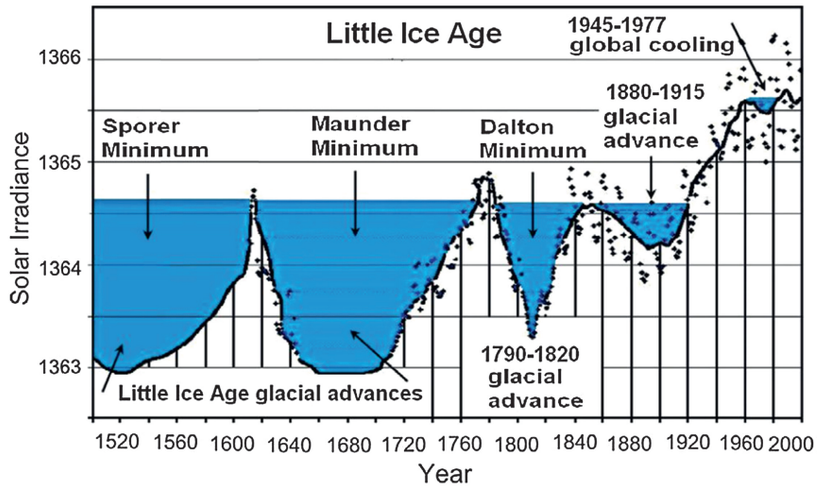

FIGURE 14.2 Relationship of solar minima, solar irradiance, and glacier advances. Blue areas were cool periods. Cool climates prevailed in all six solar minima since 1300 AD.

FIGURE 14.3 1663 painting by Jan Grifier of the frozen Thames River in London during the Maunder Minimum.

from a few to 20–30, the ground froze to several feet, alpine glaciers advanced all over the world, glaciers in the Swiss Alps encroached on farms and buried villages, tree-lines in the Alps dropped, sea ports were blocked by sea ice that surrounded Iceland and Holland for about 20 miles, wine grape harvests diminished, and cereal grain harvests failed, leading to mass famines (Fagan, 2007). The Thames River and canals and rivers of the Netherlands froze over during the winter (Fig. 14.3). The population of Iceland decreased by about half. In parts of China, warm-weather crops that had been grown for centuries were abandoned. In North America, early European settlers experienced exceptionally severe winters.

1.3.1 Sunspots

Sunspots are temporary dark spots on the surface of the sun (Fig. 14.8), where concentrations of magnetic field flux inhibit convection, reducing surface temperature. They occur in pairs and may last from a few days to a few months before eventually disappearing. Sunspots expand and contract as they move across the surface of the sun, ranging from 16 km (10 mi) to 160,000 km (100,000 mi) in diameter. Sunspots usually appear in groups. Sunspot activity cycles about every 11 years. The point of highest sunspot activity during a cycle is known as solar maximum, and the point of lowest activity as solar minimum.

FIGURE 14.4 Glaciers in the Alps advanced during the Little Ice Age.

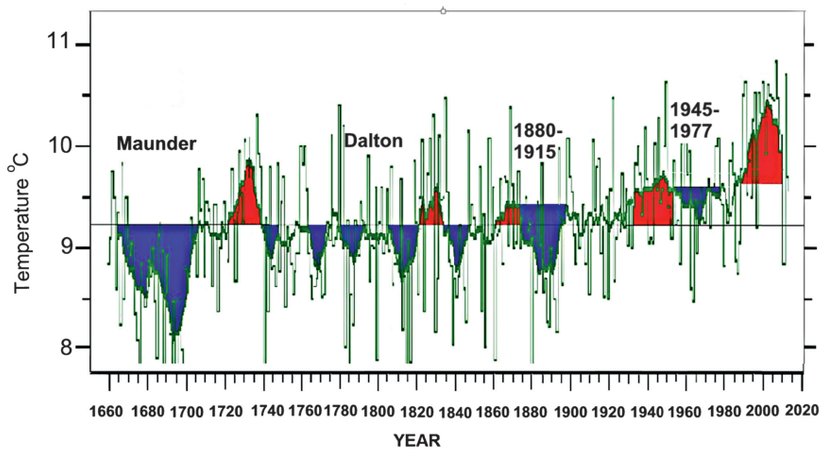

FIGURE 14.5 Central England temperatures (CET) recorded continuously since 1658. Blue areas are reoccurring cool periods; red areas are warm periods. All times of solar minima were coincident with cool periods in central England.

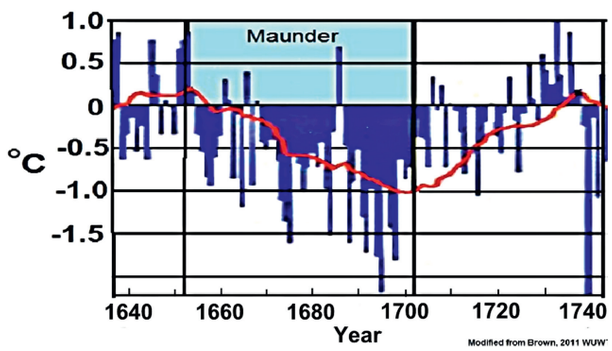

FIGURE 14.6 CET during the Maunder Minimum.

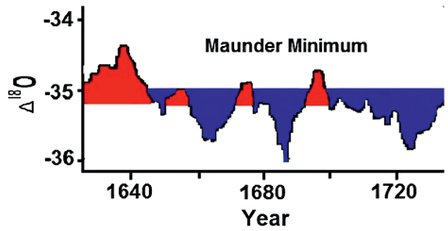

FIGURE 14.7 Oxygen isotope record, GISP2 Greenland ice core showing the Maunder Minimum. Blue area is cool, red is warm. The isotope record shows the same cooling as the CET.

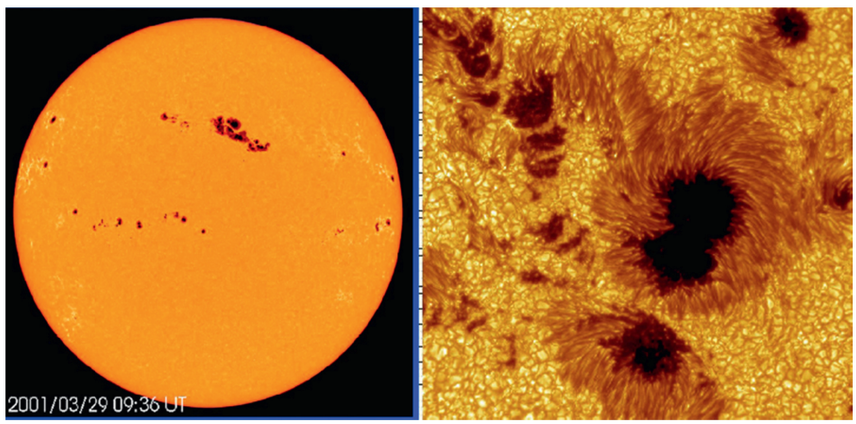

FIGURE 14.8 Sunspots. *NASA images.*

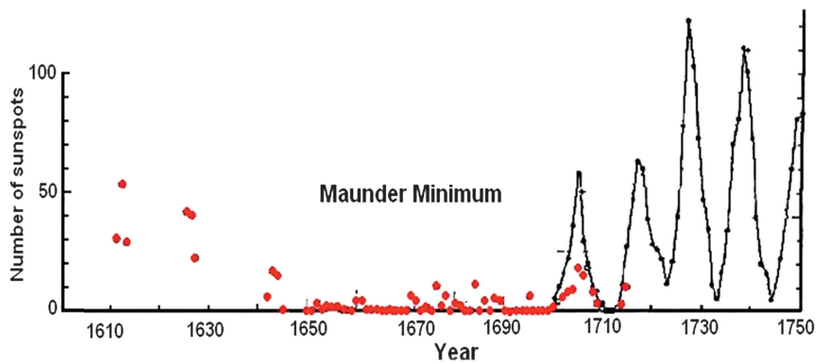

FIGURE 14.9 Sunspots during the Maunder Minimum. From 1645 to 1700, many years had no sunspots.

When Galileo perfected the telescope in 1609, scientists could see sunspots for the first time. They were of such interest that records were kept of the number of sunspots observed, and although not perfectly accurate due to cloudy days, lost records, and so on, the records show a remarkable pattern for more than a century (Fig. 14.9) (Maunder, 1894, 1922; Eddy, 1976, 1977; Soon, 2005; Hoyt and Schatten, 1997, 1998; Lean et al., 1995, 2002). From 1600 to 1715 AD, very few sunspots were seen, and from 1645 to 1715, many years had no sunspots at all, despite the fact that many scientists with telescopes were actively looking for them. The longest known minimum (about 50 years) of virtually no sunspots occurred during the Maunder Minimum. After 1715 AD, the number of observed sunspots increased sharply from near zero to 50–100 (Fig. 14.9) and the global climate warmed.

1.3.2 Total Solar Irradiance

TSI is the solar radiative power per unit area incident on the Earth's upper atmosphere. It is usually measured in watts per square meter (W/m^2). It has varied historically, reaching maximums during periods of high sunspot numbers and minimums during of low sunspot numbers (Fig. 14.10). TSI drops to lowest values during Solar Minimums and during sunspots lows.

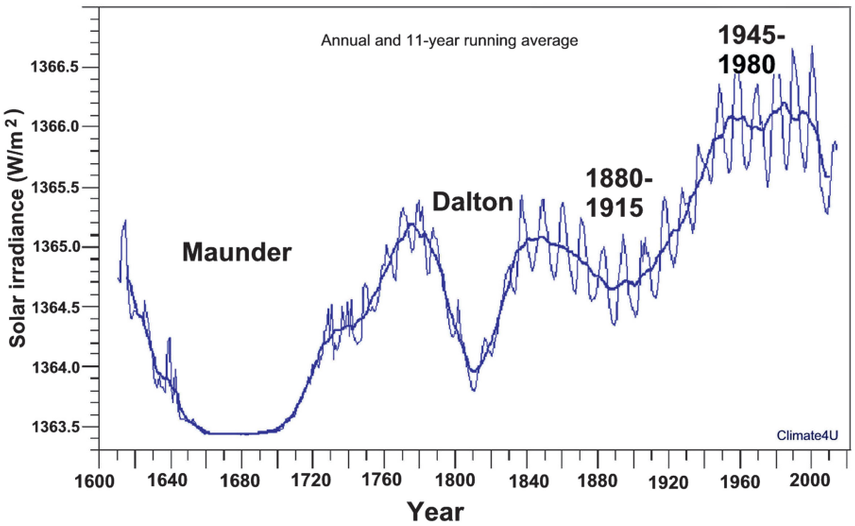

FIGURE 14.10 Total solar irradiance from 1600 to 2014 AD. *Modified from Lean, J.L., Beer, J., Bradley, R., 1995, Reconstruction of solar irradiance since 1610: implications for climatic change. Geophysics Research Letters 22, 3195–3198.*

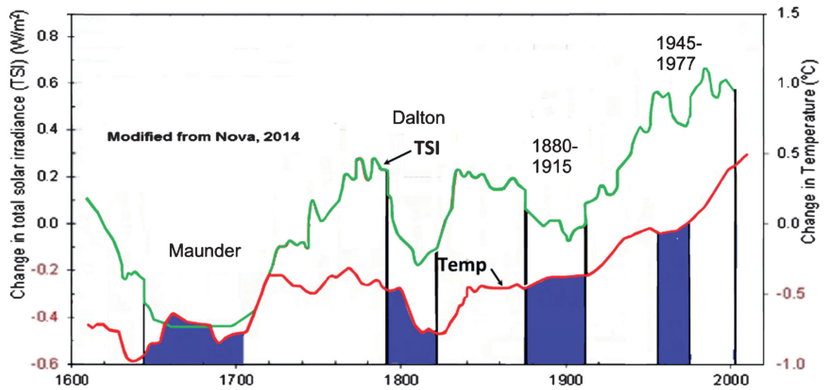

FIGURE 14.11 Correlation of total solar irradiance (TSI) and temperature. *Modified from Nova, 2014.*

1.3.3 Temperature, Sunspots, and Total Solar Irradiance

Temperatures during the Maunder closely correlate with SSNs and TSI (Fig. 14.11). When SSNs and TSI are low, temperatures are also low, and when SSNs and TSI are high, temperatures are high.

1.4 Dalton Minimum

The Dalton Minimum was a period of low SSNs and TSI from about 1790 to 1820. Like the Maunder, it was a time of intense cooling and great hardship, although not as bad as the Maunder. Widespread famines due to crop failures spread across Europe. Several notable events occurred during the Dalton, including the French Revolution and Napoleon's defeat in Russia because of a bitterly cold winter.

The cool temperatures of the Dalton show up both in the CET and GISP2 Greenland ice core (Figs. 14.12 and 14.13).

1.4.1 Sunspots

Sunspots declined sharply during the Dalton Minimum (Fig. 14.14).

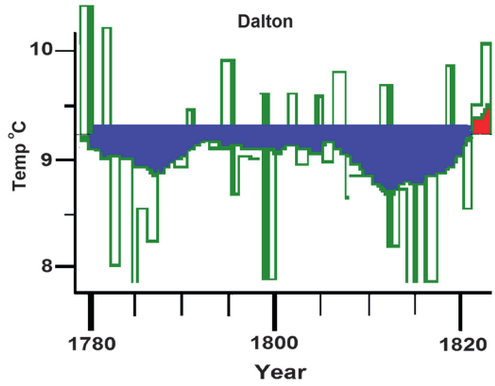

FIGURE 14.12 CET during the Dalton Minimum.

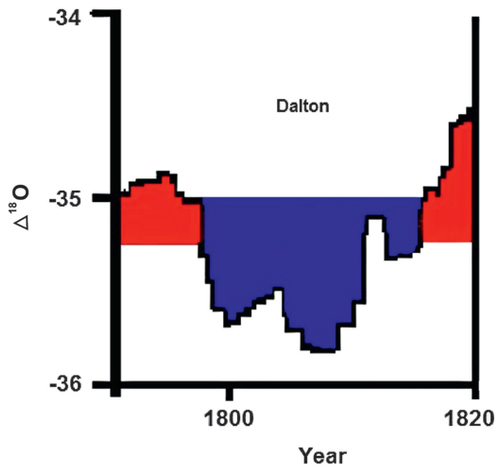

FIGURE 14.13 Oxygen isotope record from the GISP2 Greenland ice core. *Data from Grootes and Stuiver.*

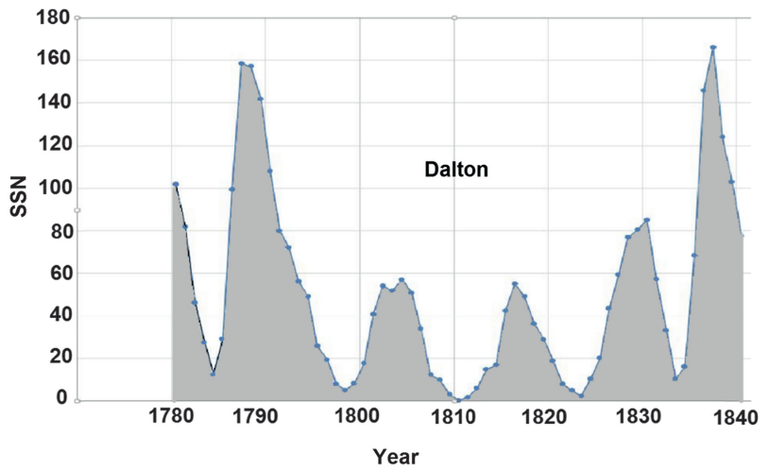

FIGURE 14.14 Sunspots during the Dalton Minimum. *Plotted from Svalgaard data.*

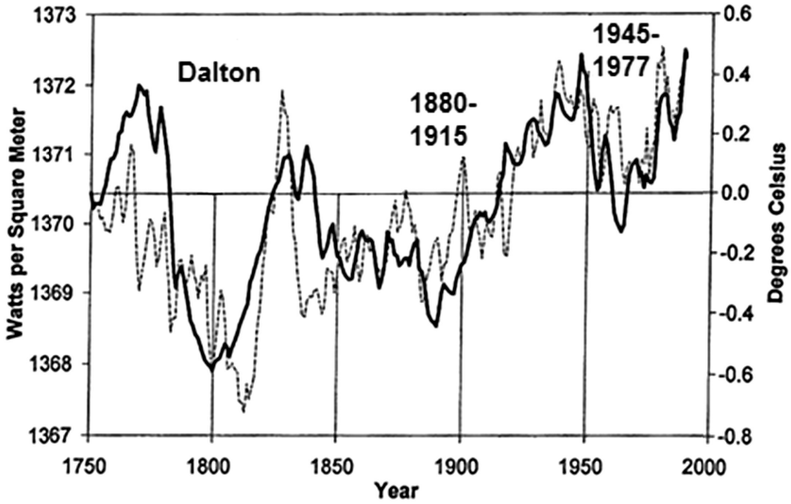

FIGURE 14.15 Solar irradiance and global temperature from 1750 to 1990. During this 250-year period, temperature and total solar irradiance curves follow a remarkably similar pattern. *Modified from Hoyt, D.V., Schatten, K.H., 1997, The Role of the Sun in Climate Change: Oxford University, p. 279.*

1.4.2 Total Solar Irradiance

TSI also declined sharply during the Dalton Minimum (Fig. 14.10).

1.4.3 Temperature and Total Solar Irradiance

During the Dalton Minimum, temperatures dropped, closely following TSI (Fig. 14.15).

1.5 1880–1915 Minimum

Temperatures dropped sharply beginning about 1880, and the 1850–1880 warm period came to a close and the climate cooled (Figs. 14.16–14.18). Alpine glaciers advanced down valley to terminal positions not far from their maximums during the early part of the LIA.

1.5.1 Sunspots

The number of sunspots declined during the 1880–1915 cool period (Fig. 14.19).

1.5.2 Total Solar Irradiance and Temperature

TSI declined during the 1880–1915 cool period (Fig. 14.10). Temperature closely followed TSI (Fig. 14.20).

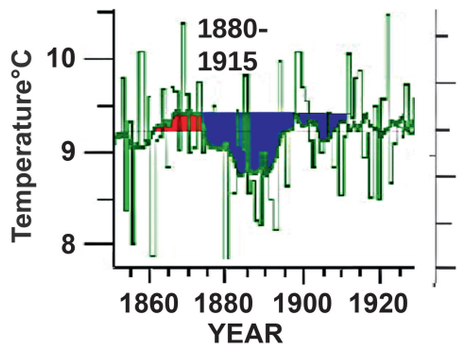

FIGURE 14.16 CET during the 1880–1915 cool period.

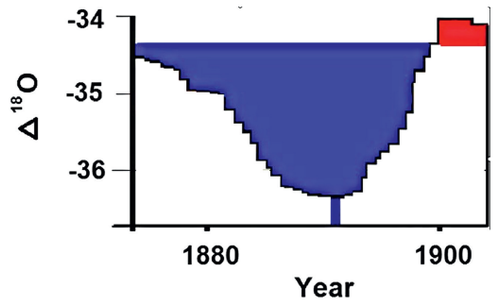

FIGURE 14.17 Oxygen isotope record from the GISP2 Greenland ice core. Blue area is cool. *Data from Grootes, P.M., Stuiver, M., 1997. Oxygen 18/16 variability in Greenland snow and ice with 10^3 to 10^5-year time resolution: Journal of Geophysical Research 102, 26455–26470.*

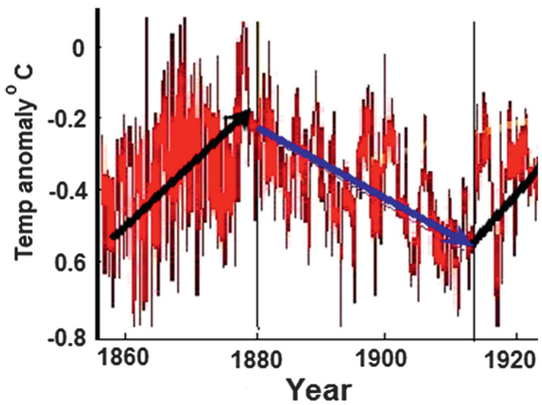

FIGURE 14.18 Global temperature, 1880 to 1915 cool period. *Modified from HADRUT3.*

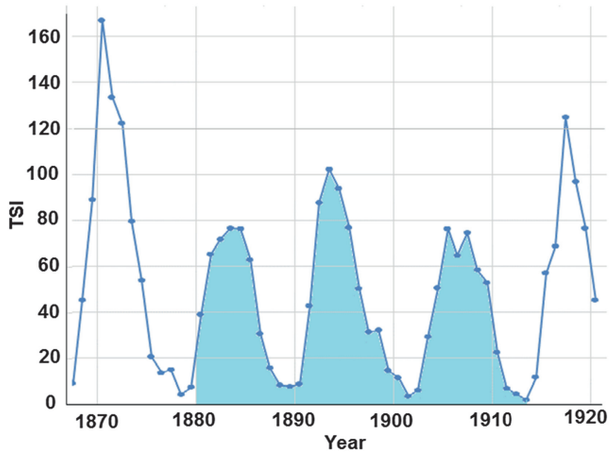

FIGURE 14.19 Sunspots during the 1880–1915 cool period.

1.6 1945–1977 Minimum

Following the early 20th-century warm period (1915–1945), the climate cooled for 30 years (Figs. 14.21 and 14.22).

1.6.1 Sunspots

The number of sunspots declined during the 1945–1977 cool period (Fig. 14.23).

1.6.2 Total Solar Irradiance and Temperature

Decline in TSI coincided with 30 years of global cooling temperatures from 1945 to 1977 (Fig. 14.20), even as CO_2 emissions soared.

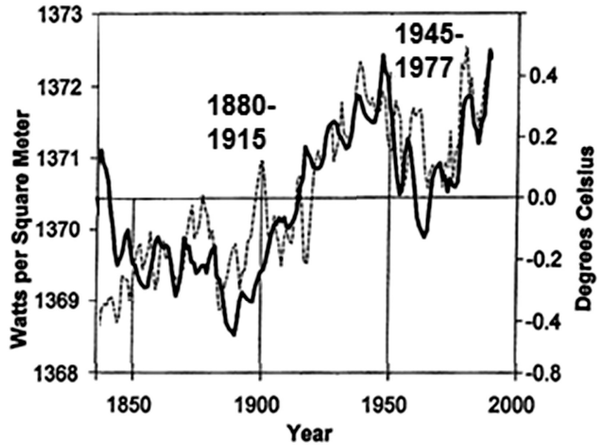

FIGURE 14.20 Total solar irradiance and temperature during the 1880–1915 cool period.

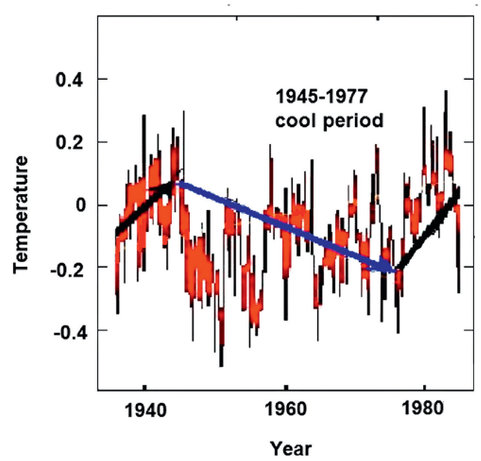

FIGURE 14.21 Temperature during the 1945–1977 cool period. *HADCRUT3.*

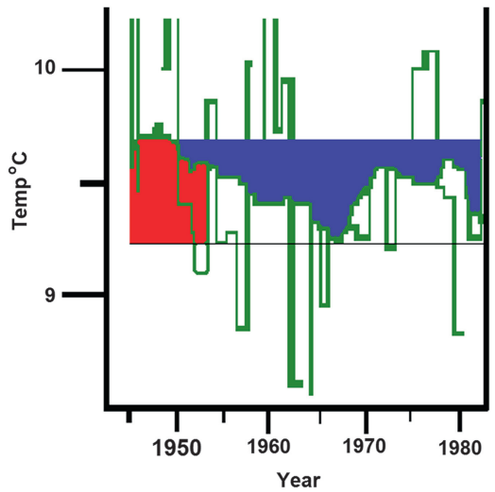

FIGURE 14.22 CET during the 1945–1977 cool period. (Blue = cool, red = warm.)

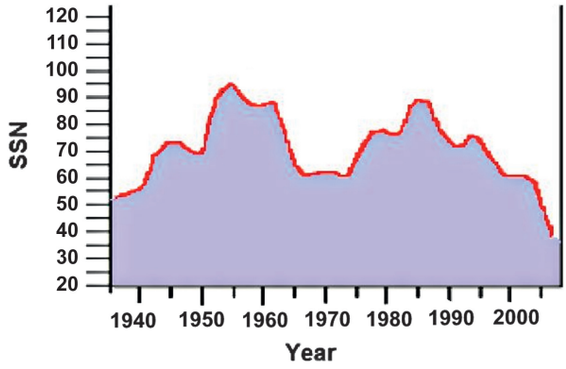

FIGURE 14.23 SSNs during the 1945–1977 cool period.

2. RADIOCARBON ($^{14}C_6$) PRODUCTION RATES

Radiocarbon ($^{14}C_6$) is produced in the upper atmosphere by collision of neutrons with nitrogen atoms ($^{14}N_7$), which has the effect of knocking a proton out the nucleus of the nitrogen atoms, thus decreasing the atomic number by one to form $^{14}C_6$:

$$^{14}N_7 + n = {}^{14}C_6 + {}^{1}H_1$$

Radiocarbon ($^{14}C_6$) differs from $^{12}C_6$, the most abundant isotope of carbon, in that its mass is greater (14 compared to 12) and its nucleus is radioactive, emitting a beta particle and an electron anti-neutrino. As a result, one of the neutrons in the $^{14}C_6$ decays to a proton, thus increasing the atomic number by 1 to form $^{14}N_7$. The half–life of the radioactive decay is 5730 years:

$$^{14}C_6 = {}^{14}N_7 + \beta-$$

Radiocarbon readily combines with oxygen to form carbon dioxide (CO_2), which mixes with other CO_2 in the atmosphere to produce a constant ratio of radioactive ^{14}C to stable ^{12}C in carbon dioxide.

Nitrogen is so abundant in the atmosphere that the amount of radiocarbon produced by this reaction is nearly equal to the number of neutrons generated by cosmic radiation. Thus the production rate of radiocarbon is a measure of cosmic radiation in the upper atmosphere. An important aspect of these reactions is that since the rate of production of radiocarbon depends on the incidence of cosmic radiation, if we can determine the production rate of ^{14}C, we can use radiocarbon as a measure of past cosmic radiation. This can be done with old tree rings, whose calendar age can be determined by counting the number of rings and the radiocarbon age can be measured by ^{14}C dating of the same ring. The amount of deviance of the ^{14}C date from the calendar age is a measure of the production rate of radiocarbon, known as $\delta^{14}C$.

Papers by Stuiver and others have shown the correlation between radiocarbon production and sunspots (Stuiver, 1961, 1994; Stuiver and Brasiunas, 1991; Stuiver and Quay, 1980; Stuiver et al., 1991, 1995). Fig. 14.24 shows changes in radiocarbon production rates ($\delta^{14}C$) since 1600 AD. $\delta^{14}C$ was higher in both the Maunder and Dalton Solar Minimums.

Figs. 14.25–14.27 show the correlation of radiocarbon production rates and temperature. Note how closely temperatures follow radiocarbon production rates and that the Wolf, Sporer, Maunder, and Dalton Solar Minimums are all characterized by high radiocarbon production rates, ie, higher incoming cosmic radiation.

3. BERYLLIUM-10 ($^{10}BE_4$) PRODUCTION RATES

$^{10}Be_4$ is a radioactive isotope of the most common beryllium, $^{9}Be_4$, formed by cosmic ray spallation of oxygen in the atmosphere (Figs. 14.28–14.30). It decays by beta decay to boron-10 with a half-life of 1.39×10^6 years. Like radiocarbon, because ^{10}Be is produced in the atmosphere by cosmic radiation, it can also be used to measure the incidence of cosmic radiation. ^{10}Be is soluble in atmospheric precipitation and accumulates in glacial ice, where it is preserved and can be measured and dated by counting annual ice layers. Good correlation between ^{14}C and ^{10}Be fluxes

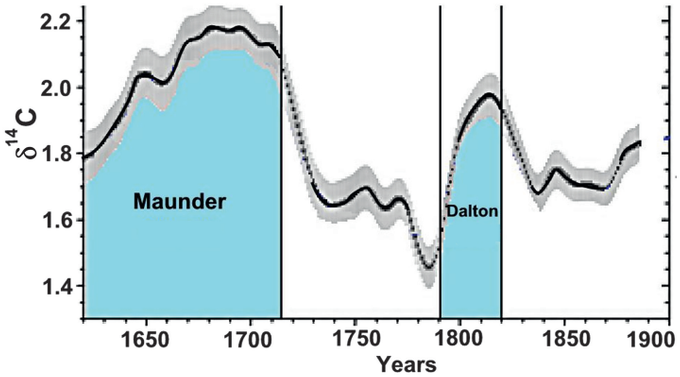

FIGURE 14.24 $\delta^{14}C$ changes since 1600 AD. Note the high values during the Maunder and Dalton Solar Minimums.

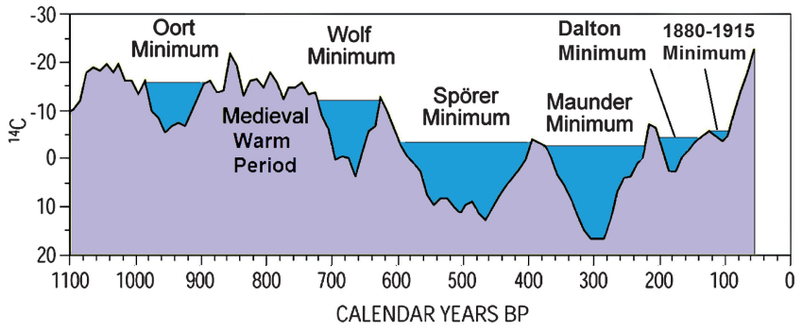

FIGURE 14.25 Correlation of ^{14}C with Oort, Wolf, Sporer, Maunder, Dalton, and 1880–1915 Solar Minimums. Each solar minimum was a period of high ^{14}C production and each corresponded to a cold climate.

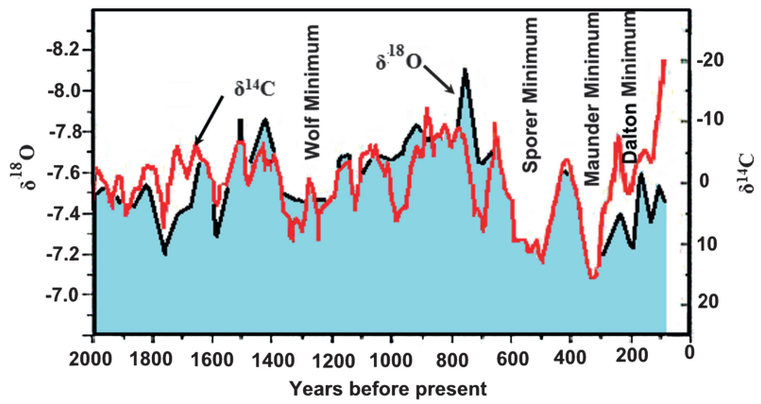

FIGURE 14.26 Correlation of temperature ($\delta^{18}O$) and radiocarbon production rates ($\delta^{14}C$). Temperature closely follows radiocarbon production rates ($\delta^{14}C$).

(Fig. 14.31) indicates that both are a result of changes in cosmic radiation, since their transport processes to their place of accumulation are so different—^{14}C is measured from tree rings and ^{10}Be is measured from glacial ice cores. The relationship of ^{10}Be to cosmic radiation is confirmed by the correlation of ^{10}Be and solar magnetic flux (Fig. 14.32).

3.1 Berylium-10 (^{10}Be) and Sunspots

Both ^{10}Be and SSNs are directly related to solar magnetism, so it is not surprising that ^{10}Be correlates well with sunspots (Fig. 14.33).

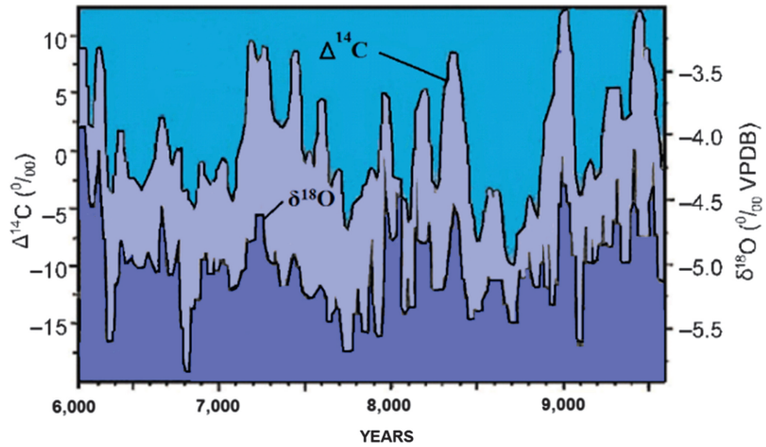

FIGURE 14.27 Close correlation of radiocarbon production ($\delta^{14}C$) and temperature ($\delta^{18}O$) from a stalagmite in Oman (Matter et al., 2001).

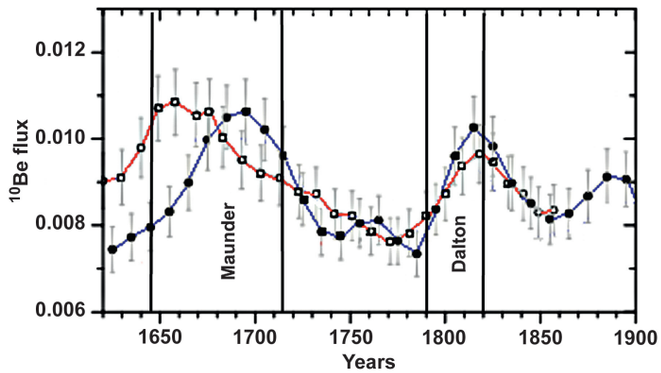

FIGURE 14.28 Depositional flux of ^{10}Be in ice cores in Greenland (red) and Antarctica (blue). Note the high ^{10}Be values during the Maunder and Dalton Solar Minimums. *Modified from Usoskin, I.G., et al., 2015. The Maunder minimum (1645–1715) was indeed a grand minimum: a reassessment of multiple datasets. Astronomy Astrophysics 581, 1–19.*

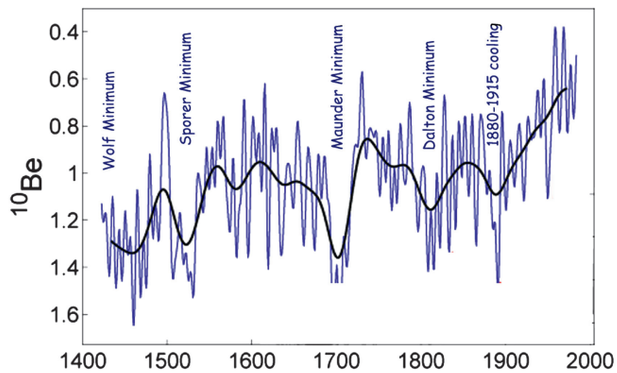

FIGURE 14.29 Fluctuation of ^{10}Be as a measure of cosmic ray incidence. Note that ^{10}Be production rates were high for the Wolf, Sporer, Maunder, Dalton, and 1880–1915 solar minima.

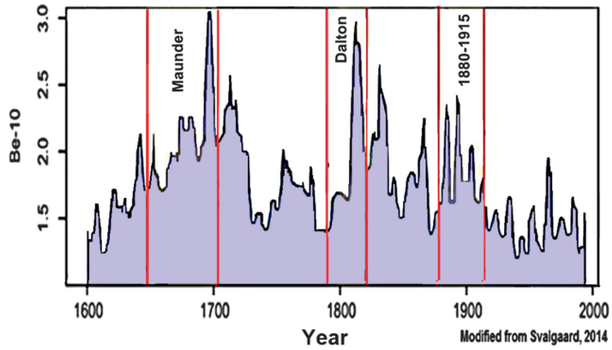

FIGURE 14.30 ^{10}Be production was higher during the Maunder, Dalton, and 1880–1915 Solar Minimums, indicating that cosmic ray incidence was higher then. *Modified from Svalgaard.*

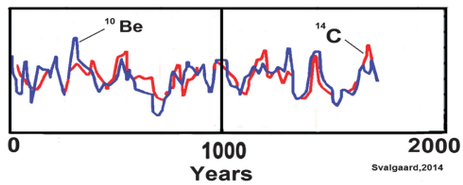

FIGURE 14.31 ^{10}Be and ^{14}C fluxes over the past 2000 years show good correlation, despite having very different paths of accumulation. *Modified from Svalgaard.*

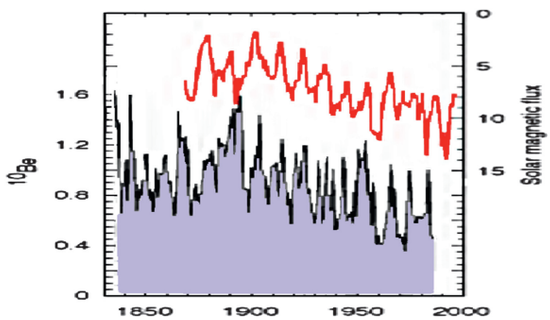

FIGURE 14.32 Variation of ^{10}Be concentration in Greenland ice cores and the solar magnetic field derived from geomagnetic measurements. *Modified from Kirkby, J., 2008. Cosmic rays and climate. Surveys in Geophysics 28, 5.*

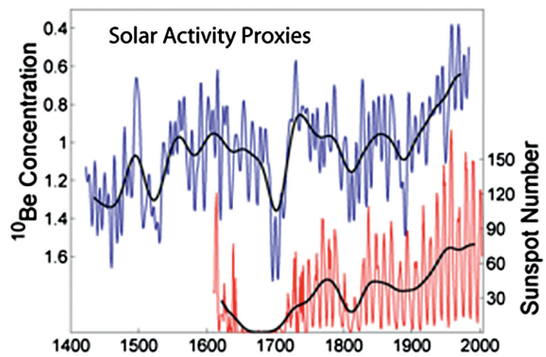

FIGURE 14.33 Correlation of ^{10}Be concentration from the Dye-3 Greenland ice core and SSNs. (Beer et al., 1994.)

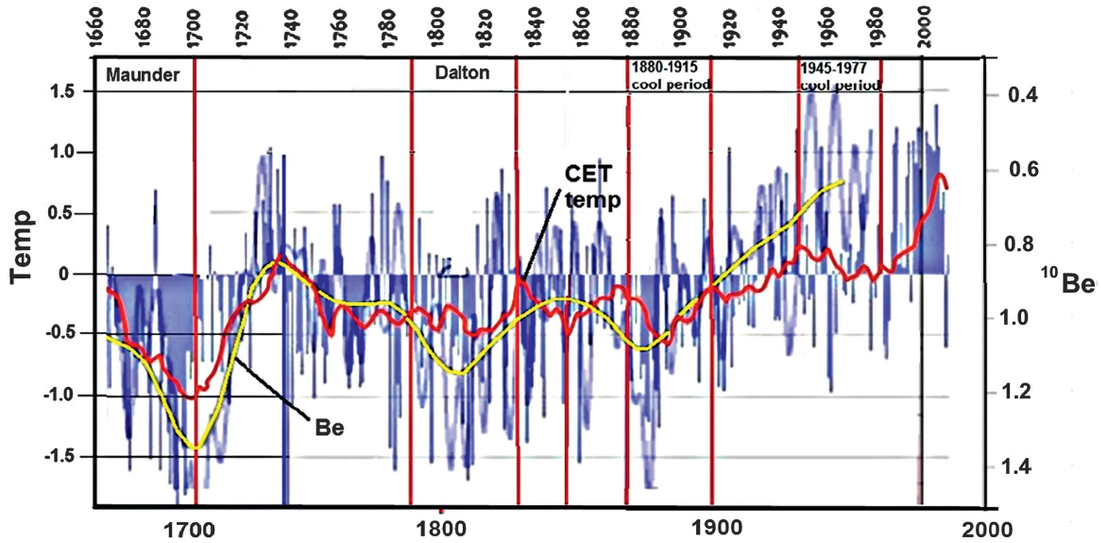

FIGURE 14.34 Correlation of ^{10}Be and temperature. Note that the Maunder, Dalton, 1880–1915, and 1945–1977 cold periods were all characterized by high rates of ^{10}Be production, indicating increased incidence of cosmic rays.

3.2 Berylium-10 (^{10}Be) Production and Temperature

Fig. 14.34 shows that high production rates of ^{10}Be occurred during the Maunder, Dalton, 1880–1915, and 1945–1977 cold periods, indicating higher incidence of cosmic rays during the cold episodes.

4. COSMIC RAY INCIDENCE AND CLIMATE

Studies of the effects of cosmic radiation on the atmosphere date back to the 1912 development of the Wilson cloud chamber by C.T.R. Wilson, who showed that cosmic radiation would create trails of condensation in water-saturated air. The role of cosmic rays in climate change was suggested by Ney (1959) and by Dickinson (1975), and more recently by Svensmark (2006), Svensmark and Calder (2007), Svensmark and Friis-Christensen (1997), Svensmark et al. (2007), Usoskin et al. (2004a,b), Kirkby (2008), Marsh and Svensmark (2000), and others.

Cosmic rays consist of two types of high-energy radiation: (1) galactic cosmic rays (GCRs), high–energy particles originating outside the solar system; and (2) high-energy particles (mostly protons) emitted by the sun during solar events. They may produce showers of secondary particles that penetrate and impact the Earth's atmosphere. About 99% of primary cosmic rays entering the Earth's atmosphere are nuclei of atoms; about 90% are simple protons and 9% alpha particles. About 1% consists of electrons.

High-energy protons passing through the atmosphere cause ionization and produce nuclei for condensation of water droplets. Condensation tends to occur readily in the atmosphere because it is often supersaturated with water vapor. Clouds reflect incoming solar irradiance, which results in atmospheric cooling. Clouds account for about 28 Wm^{-2} of global cooling, so even small changes in cloud cover can have a significant effect on climate. Low-altitude, layered clouds covering large areas are most effective in reflecting incoming solar radiation and make the greatest contribution to atmospheric cooling. Cosmic-ray-produced clouds may provide the key to understanding global climate. Increased cosmic ray flux creates clouds, which increase albedo and results in global cooling (Fig. 14.35). This mechanism explains the observed synchronicity of global climate changes, abrupt climate reversals, and climate changes on all time scales. Thus, cloud-generating cosmic rays provide a satisfactory explanation for both long-term and short-term climate changes (Easterbrook, 2001, 2005, 2006a,b, 2007, 2008a,b,c, 2009, 2011a,b, 2014).

As discussed above, cosmic rays produce radiocarbon and berylium–10 isotopes in the upper atmosphere in amounts proportional to the incidence of incoming radiation. This is reflected in the coincidence of ^{14}C and ^{10}Be production rates (Fig. 14.36).

Fig. 14.37 summarizes the relationships between low solar magnetic field, sunspots, galactic cosmic rays, cloud formation, albedo, and global cooling.

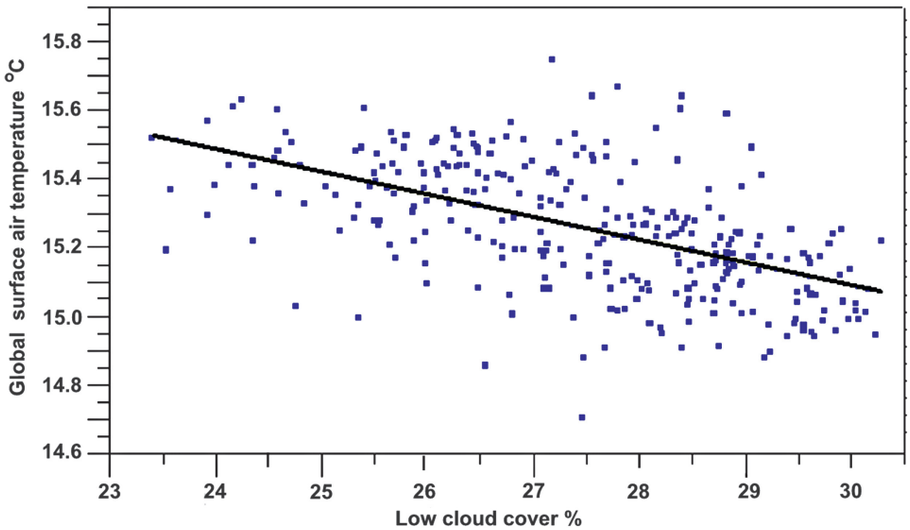

FIGURE 14.35 Global atmospheric cooling by increasing cloud cover. As cloud cover increases, temperatures decline.

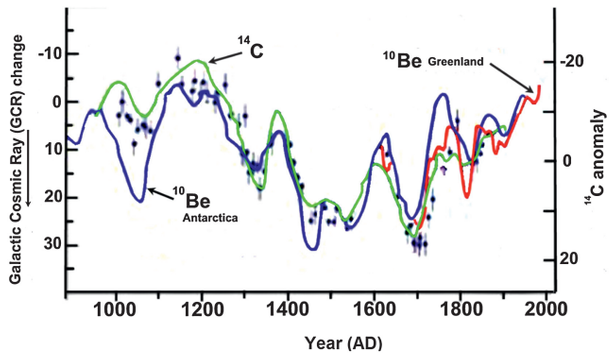

FIGURE 14.36 Correlation of ^{14}C and ^{10}Be production rates for the past 1000 years. *Modified from Kirkby, J., 2008. Cosmic rays and climate. Surveys in Geophysics 28, 5.*

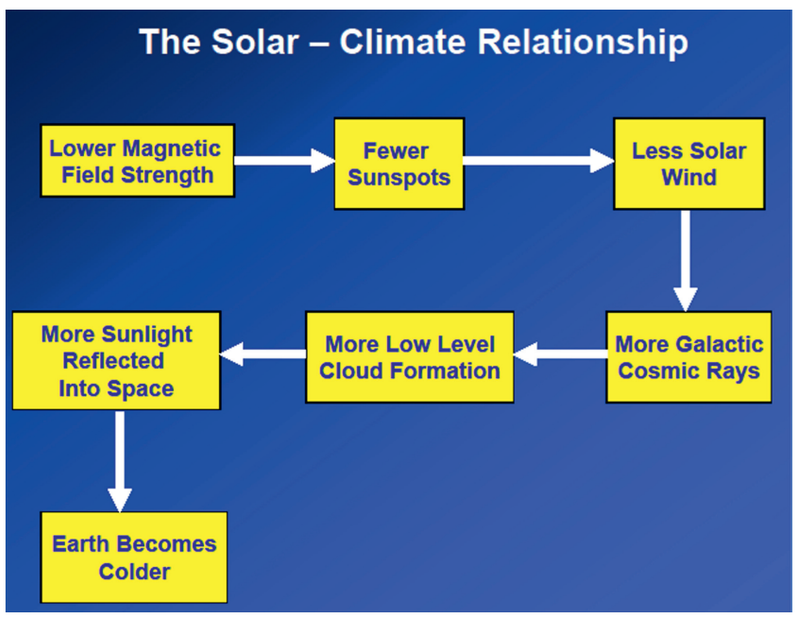

FIGURE 14.37 Relationship of low solar magnetic field, sunspots, galactic cosmic rays, cloud formation, and albedo in causing global cooling.

5. CONCLUSIONS

Excellent correlations can be made between global temperature change, sunspots, TSI, ^{14}C and ^{10}Be production in the upper atmosphere, cosmic ray incidence, and albedo from cloud generation. Global cooling coincided with changes in sunspot activity, TSI, solar flux, cosmic ray incidence, and rates of production of ^{14}C and ^{10}Be in the upper atmosphere during the Oort, Wolf, Maunder, Dalton, 1880–1915, and 1945–1977 Solar Minimums. Increased ^{14}C and ^{10}Be production during times of increased cosmic radiation serve as a proxy for solar activity.

Ionization in the atmosphere caused by cosmic rays causes increased cloudiness that reflects incoming sunlight and cools the Earth. The amount of cosmic radiation is greatly affected by the sun's magnetic field, so during times of weak solar magnetic field, more cosmic radiation reaches the Earth, creating more cloudiness and cooling the atmosphere.

This mechanism accounts for the global synchronicity of climate changes, abrupt climate reversals, and climate changes on all time scales. Thus, cloud-generating cosmic rays provide a satisfactory explanation for both long-term and short-term climate changes.

References

Beer, J., Joos, F., Lukasczyk, C., Mende, W., Rodriguez, J., Sikegenthaler, U., Stellmacher, R., 1994. ^{10}Be as an indicator of solar variability and climate. In: Nesme-Ribes, E. (Ed.), The Solar Engine and Its Influence on Terrestrial Atmosphere and Climate. Springer–Verlag, Berlin, pp. 221–233.

Dickinson, R.E., 1975. Solar variability and the lower atmosphere. Bulletin of American Meteorological Society 56, 1240.

Easterbrook, D.J., 2001. The next 25 years: global warming or global cooling? Geologic and oceanographic evidence for cyclical climatic oscillations. Geological Society of America 33, 253. Abstracts with Program.

Easterbrook, D.J., 2005. Causes and effects of abrupt, global, climate changes and global warming. Geological Society of America 37, 41. Abstracts with Program.

Easterbrook, D.J., 2006a. Causes of abrupt global climate changes and global warming predictions for the coming century. Geological Society of America 38, 77. Abstracts with Program.

Easterbrook, D.J., 2006b. The cause of global warming and predictions for the coming century. Geological Society of America 38, 235–236. Abstracts with Program.

Easterbrook, D.J., 2007. Geologic evidence of recurring climate cycles and their implications for the cause of global warming and climate changes in the coming century. Geological Society of America 39, 507. Abstracts with Programs.

Easterbrook, D.J., 2008a. Solar influence on recurring global, decadal, climate cycles recorded by glacial fluctuations, ice cores, sea surface temperatures, and historic measurements over the past millennium. In: Abstracts of American Geophysical Union Annual Meeting, San Francisco.

Easterbrook, D.J., 2008b. Implications of glacial fluctuations, PDO, NAO, and sun spot cycles for global climate in the coming decades. Geological Society of America 40, 428. Abstracts with Programs.

Easterbrook, D.J., 2008c. Correlation of climatic and solar variations over the past 500 years and predicting global climate changes from recurring climate cycles. In: Abstracts of 33rd International Geological Congress, Oslo, Norway.

Easterbrook, D.J., 2009. The role of the oceans and the sun in late Pleistocene and historical glacial and climatic fluctuations. Geological Society of America 41, 33. Abstracts with Programs.

Easterbrook, D.J., 2011a. Geologic evidence of recurring climate cycles and their implications for the cause of global climate changes: the past is the key to the future. In: Evidence-based Climate Science. Elsevier Inc, pp. 3–51.

Easterbrook, D.J., 2011b. Climatic implications of the impending grand solar minimum and cool Pacific Decadal Oscillation: the past is the key to the future–what we can learn from recurring past climate cycles recorded by glacial fluctuations, ice cores, sea surface temperatures, and historic measurements. Geologic Society of America 43, 34. Abstracts with Programs.

Easterbrook, D.J., 2014. Synchroneity of multiple Younger Dryas and Allerod moraines in the Fraser Lowland with late Pleistocene moraines in North America, Europe, New Zealand, and South America. Geological Society of America 46, 349. Abstracts with Programs.

Eddy, J.A., 1976. The Maunder Minimum. Science 192, 1189–1202.

Eddy, J.A., 1977. Climate and the changing sun. Climatic Change 1, 173–190.

Fagan, B., 2000. The Little Ice Age. Basic Books, N.Y., p. 246.

Fagan, B., 2007. The Great Warming: Climate Change and the Rise and Fall of Civilizations. Bloomsbury Press, p. 283.

Grootes, P.M., Stuiver, M., 1997. Oxygen 18/16 variability in Greenland snow and ice with 10^3 to 10^5-year time resolution. Journal of Geophysical Research 102, 26455–26470.

Grove, J.M., 2004. Little Ice Ages: Ancient and Modern. Routledge, London, p. 718.

Hoyt, D.V., Schatten, K.H., 1997. The Role of the Sun in Climate Change. Oxford University, p. 279.

Hoyt, D.V., Schatten, K.H., 1998. Group sunspot numbers: a new solar activity reconstruction. Solar Physics 179, 189–219.

Kirkby, J., 2008. Cosmic rays and climate. Surveys in Geophysics 28, 5.

Lean, J.L., Beer, J., Bradley, R., 1995. Reconstruction of solar irradiance since 1610: implications for climatic change. Geophysics Research Letters 22, 3195–3198.

Lean, J.L., Wang, Y.M., Sheeley, N.R., 2002. The effect of increasing solar activity on the Sun's total and open magnetic flux during multiple cycles: implications for solar forcing of climate. Geophysics Research Letters 29, 2224.

Marsh, N.D., Svensmark, H., 2000. Low cloud properties influenced by cosmic rays. Physics Revue Letters 85, 5004–5007.

Matter, A., Neff, U., Fleitmann, D., Burns, S., Mangini, A., 2001. 350,000 years of climate variability recorded in speleothems from Oman. GeoArabia (Manama) 6, 315–316.
Maunder, E.W., 1894. A prolonged sunspot minimum. Knowledge 17, 173–176.
Maunder, E.W., 1922. The prolonged sunspot minimum, 1645–1715. Journal of the British Astronomical Society 32, 140.
Ney, E.P., 1959. Cosmic radiation and the weather. Nature 183, 451–452.
Soon, W., 2005. Variable solar irradiance as a plausible agent for multidecadal variations in the Arctic–wide surface air temperature record of the past 130 years. Geophysical Research Letters 32, L16712.
Stuiver, M., 1961. Variations in radio carbon concentration and sunspot activity. Geophysical Research 66, 273–276.
Stuiver, M., 1994. Atmospheric ^{14}C as a proxy of solar and climatic change. In: Nesme-Ribes (Ed.), The Solar Engine and Its Influence on Terrestrial Atmosphere and Climate. Springer–Verlag, Berlin, pp. 203–220.
Stuiver, M., Brasiunas, T.F., 1991. Isotopic and solar records. In: Bradley, R.S. (Ed.), Global Changes of the Past. Boulder University, Corporation for Atmospheric Research, pp. 225–244.
Stuiver, M., Quay, P.D., 1980. Changes in atmospheric carbon-14 attributed to a variable Sun. Science 207, 11–19.
Stuiver, M., Grootes, P.M., Brasiunas, T.F., 1995. The GISP2 $d^{18}O$ record of the past 16,500 years and the role of the sun, ocean, and volcanoes. Quaternary Research 44, 341–354.
Stuiver, M., Braziunas, T.F., Becker, B., Kromer, B., 1991. Climatic, solar, oceanic, and geomagnetic influences on late-glacial and Holocene atmospheric $^{14}C/^{12}C$ change. Quaternary Research 35, 1–24.
Svensmark, H., 2006. Imprint of galactic dynamics on Earth's climate. Astronomische Nachrichten 327, 866–870.
Svensmark, H., Calder, N., 2007. The Chilling Stars: A New Theory of Climate Change. Icon Books, Allen and Unwin Pty Ltd, p. 246.
Svensmark, H., Friis-Christensen, E., 1997. Variation of cosmic ray flux and global cloud cover–a missing link in solar–climate relationships. Journal of Atmospheric and Solar–Terrestrial Physics 59, 1125–1132.
Svensmark, H., Pedersen, J.O., Marsh, N.D., Enghoff, M.B., Uggerhøj, U.I., 2007. Experimental evidence for the role of ions in particle nucleation under atmospheric conditions. Proceedings of the Royal Society 463, 385–396.
Usoskin, I.G., Marsh, N.D., Kovaltsov, G.A., Mursula, K., Gladysheva, O.G., 2004a. Latitudinal dependence of low cloud amount on cosmic ray induced ionization. Geophysis Research Letters 31, L16109. http://dx.doi.org/10.1029/2004GL019507.
Usoskin, I.G., Mursula, K., Solanki, S.K., Schussler, M., Alanko, K., 2004b. Reconstruction of solar activity for the last millenium using ^{10}Be data. Astronomy and Astrophysics 413, 745–751.
Usoskin, I.G., et al., 2015. The Maunder minimum (1645–1715) was indeed a grand minimum: a reassessment of multiple datasets. Astronomy Astrophysics 581, 1–19.